Journal of Electrical and Computer Engineering Innovations
(JECEI)
Journal homepage: http://www.jecei.sru.ac.ir

Research paper

# Coordinated Model Predictive DC-Link Voltage, Current, and Electromagnetic Torque Control of Wind Turbine with DFIG under Grid Faults

*Z. Dehghani Arani[1], S.A. Taher[1,*], M.H. Karimi[1,2], M. Rahimi[1]*
[1]*Department of Electrical Engineering, University of Kashan, Kashan, Iran.*
[2]*Iranian Oil Pipeline and Telecommunication Company, Iran.*

**Article Info**

**Article History:**
Received 23 October 2019
Reviewed 11 December 2019
Revised 01 January 2020
Accepted 02 March 2020

**Keywords:**
Coordinated model predictive control
DFIG-based WT
Grid code requirements
Grid faults

[*]Corresponding Author's Email Address:
*ataher@kashanu.ac.ir*

**Abstract**

**Background and Objectives:** The wind turbines (WTs) with doubly fed induction generator (DFIG) have active and reactive power as well as electromagnetic torque oscillations, rotor over-current and DC-link over-voltage problems under grid faults. Solutions for these problems presented in articles can be classified into three categories: hardware protection devices, software methods, and combination of hardware and software techniques.
**Methods:** Conventional protection devices used for fault ride through (FRT) capability improvement of grid-connected DFIG-based WTs impose difficulty in rotor side converter (RSC) controlling, causing failure to comply with grid code requirements. Hence, the main idea in this paper is to develop a novel coordinated model predictive control (MPC) for the power converters without need to use any auxiliary hardware. Control objectives are defined to maintain DC-link voltage, rotor current as well as electromagnetic torque within permissible limits under grid fault conditions by choosing the best switching state so as to meet and exceed FRT requirements. Model predictive current and electromagnetic torque control schemes are implemented in the RSC. Also, model predictive current and DC-link voltage control schemes are applied to grid side converter (GSC).
**Results:** To validate the proposed control method, simulation studies are compared to conventional proportional-plus-integral (PI) controllers and sliding mode control (SMC) with pulse-width modulation (PWM) switching algorithm. In different case studies comprising variable wind speeds, single-phase fault, DFIG parameters variations, and severe voltage dip, the rotor current and DC-link voltage are respectively restricted to 2 pu and 1.2 times of DC-link rated voltage by the proposed MPC-based approach. The maximum peak values of DC-link voltage are 1783, 1463 and 1190 V by using PI control, SMC and the proposed methods, respectively. The maximum peak values of rotor current obtained by PI control, SMC and the proposed strategies are 3.23, 3.3 and 1.95 pu, respectively. Also, PI control, SMC and the proposed MPC methods present 0.8, 0.4 and 0.14 pu, respectively as the maximum peak values of electromagnetic torque.
**Conclusion:** The proposed control schemes are able to effectively improve the FRT capability of grid-connected DFIG-based WTs and keep the values of DC-link voltage, rotor current and electromagnetic torque within the acceptable limits. Moreover, these schemes present fast dynamic behavior during grid fault conditions due to modulator-free capability of the MPC method.



## Introduction

Due to development in power electronic technology, variable speed wind energy conversion systems (WECSs)

are integrated into power systems [1]. Among different types of WECSs, doubly fed induction generator (DFIG)-based wind turbines (WTs) are widely used because of flexible operation at different speeds, high energy transfer capability, requirement of low cost and small size power electronics system, control capability of active and reactive powers, etc. [2].

During faults and voltage dips occurred in a power grid, the stator current of DFIG-based WT increases as a result of the direct connection of stator windings to the power grid. Since there is magnetic coupling between stator and rotor windings, high rotor inrush currents and DC-link capacitor over-voltage are created [3]. In order to address the risk of damage to rotor side converter (RSC) and DC-link capacitor, and to improve the fault ride through (FRT) capability, researchers have proposed three different types of solutions: hardware protection techniques, software methods, and combination of hardware and software methods.

Crowbar is an old hardware protection device to maintain power electronics and to improve FRT behavior of DFIG-based WTs. It suggests disconnecting WT from the grid during severe electrical faults. Although this protection device avoids high rotor inrush currents and leads to RSC isolation, the DFIG-based WT operates similar to a squirrel cage induction generator drawing a considerable amount of reactive power from the power grid [4], [5]. On the other hand, recent grid codes require DFIG-based WTs to stay connected to the power grid during and after faults, and to provide FRT capability [6]. Therefore, developed control strategies have been proposed to improve the DFIG performance during the voltage dip and crowbar activation [7], [8].

A set of thyristor controlled resistors that are connected to the rotor windings have been presented in [3] in order to limit the high current and to provide a bypass for it in the rotor circuit. Furthermore, superconducting magnetic energy storage-fault current limiter (SMES-FCL) [9], dynamic voltage restorer (DVR) [10], static synchronous compensator (STATCOM) [11] and static volt ampere reactive compensator (SVC) [12] are employed as hardware protection methods to improve FRT behavior of DFIG-based WTs. In [13], the authors used a superconducting coil (SC) in the DFIG-based WT's DC-link. The proposed hardware solution acts as a FCL during severe faults of power systems to reduce the rotor and stator over-currents and also the DC-link over-voltage, while it acts as an energy storage device during normal operating conditions to smooth out output power fluctuations. FRT requirement of current-based protection devices which their accurate operation necessitates fault current provision by resources for a given period of time has been discussed in [14]. In [15], a modified DC chopper has been proposed not only to keep the DC-link voltage in acceptable range, but also to limit the rotor transient over-current in a permissible level without requiring the high rated current antiparallel diodes in the RSC. A novel inductive superconducting fault current limiter (SFCL)-based protection strategy with demagnetization technology has been presented in [16] to enhance the FRT capability of DFIG-based WTs. However, hardware solutions are still expensive as well as, they impose additional maintenance costs.

In addition to hardware protection techniques, advanced control strategies have been introduced to limit the DC-link over-voltage and rotor over-current which might be categorized under software solutions [17]-[23], [25]-[29]. The authors in [21] implemented proportional-plus-integral (PI) controllers combined with Lyapunov-based nonlinear control method in order to enhance the transient behavior of DFIG-based WT. In this FRT method, the rotor back-EMF voltage compensation leads to limit inrush current of the rotor and electromagnetic torque oscillations. In [22] and [23], feed-forward transient control approach was utilized for RSC so as to enhance the FRT capability.

In recent years, model predictive control (MPC) has attracted lots of attention because it provides a free-modulation technique to control power converters, as well as simple and flexible control approach while constraints and nonlinearities are included. In [24], a model-based predictive controller has been presented for DFIG direct power control in RSC which the control law has been derived by optimization of the difference between the predicted active and reactive powers and their references. Model predictive current control has been proposed as FRT improvement strategy for DFIG-based WT in [25]-[27].

Nevertheless, none of these works utilize the benefits of MPC to control and limit DC-link voltage and electromagnetic torque during fault conditions. An application of fuzzy logic controller with type of Takagi–Sugeno–Kang tuned using adaptive neuro-fuzzy inference system (ANFIS) and MPC theory for power converters was designed in [27] to limit the DC-link over-voltage and rotor over-current under fault conditions, although improving transient electromagnetic torque has not been considered.

As the DFIG-based WT has nonlinear dynamics, nonlinear controllers have been applied to power converters in [28], [29]. The transient behavior of DFIG by using sliding mode controllers and two protection circuits of crowbar and DC-chopper under severe grid faults was discussed in [28]. Even though the proposed nonlinear control technique can regulate DC-link voltage within acceptable limit, it tends to fail in limiting the rotor current.

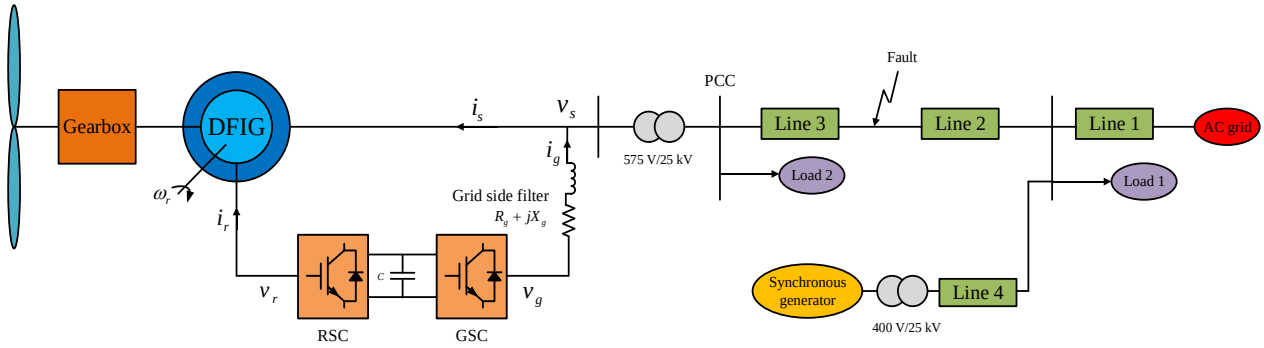


Fig. 1: The grid-connected WT with DFIG under study.

Because of high cost and low system reliability of using hardware solutions and unsatisfactory performance of some software solutions, proposing a new control approach as a software solution in order to enhance FRT capability of DFIG-based WT still seems indispensable; a novel approach which is robust against changes in the system model without requiring auxiliary protection devices. Since the PI controllers will be easily saturated under severe voltage dips, these controllers with pulse-width modulation (PWM) switching algorithm in both RSC and grid side converter (GSC) are substituting by MPC schemes in this paper. As the main contribution of this paper, predictive control of electromagnetic torque and DC-link voltage during fault condition are employed in coordinated MPC schemes of RSC and GSC, respectively. Moreover, power converter switching signals are obtained by the MPC theory without using any additional modulation techniques to improve the FRT capability of DFIG-based WTs during extreme voltage dips. And finally, the proposed control structure performance in the FRT capability enhancement of DFIG-based WTs is compared with sliding mode control (SMC) and PI control by several simulations in the MATLAB/SIMULINK environment.

The remaining parts of the paper are given as follows. The next section presents modeling and conventional control structure of DFIG-based WTs. Then, the SMC for FRT improvement, which has been proposed in [28], is reviewed. Next, the design of improved MPC-based control schemes for enhancing transient behavior of DFIG-based WT under grid fault condition is described. Simulation results are discussed and concluded in the next sections to validate the efficiency of the proposed control approach.

## Modeling and Conventional Control of DFIG-Based WT

The schematic diagram of the DFIG-based WT test system is illustrated in Fig. 1. With respect to the indicated stator and rotor current directions, the DFIG-based WT dynamics in a synchronous reference frame is derived. The voltages and also fluxes of stator and rotor circuits in a $dq$ reference frame rotating at angular speed of $\omega$, in per unit values, and referred to the stator side are presented as follows [21], [30]:

$$v_{sdq} = R_s i_{sdq} + j\omega\psi_{sdq} + \frac{1}{\omega_b}\frac{d\psi_{sdq}}{dt} \tag{1}$$

$$v_{rdq} = R_r i_{rdq} + j\omega_2\psi_{rdq} + \frac{1}{\omega_b}\frac{d\psi_{rdq}}{dt} \tag{2}$$

$$\psi_{sdq} = L_s i_{sdq} + L_m i_{rdq} \tag{3}$$

$$\psi_{rdq} = L_r i_{rdq} + L_m i_{sdq} \tag{4}$$

In accordance with (1), the stator flux state space equations can be written as

$$\begin{cases} \dfrac{d\psi_{sd}}{dt} = \omega_b\left(v_{sd} - R_s i_{sd} + \omega\psi_{sq}\right) \\ \dfrac{d\psi_{sq}}{dt} = \omega_b\left(v_{sq} - R_s i_{sq} - \omega\psi_{sd}\right) \end{cases} \tag{5}$$

Using (2)-(4), the state space equations of rotor circuit are given as

$$\begin{cases} \dfrac{di_{rd}}{dt} = -\dfrac{\omega_b R_r'}{L_r'} i_{rd} + \omega_b\omega_2 i_{rq} - \dfrac{\omega_b}{L_r'} E_d + \dfrac{\omega_b}{L_r'} v_{rd} \\ \dfrac{di_{rq}}{dt} = -\dfrac{\omega_b R_r'}{L_r'} i_{rq} - \omega_b\omega_2 i_{rd} - \dfrac{\omega_b}{L_r'} E_q + \dfrac{\omega_b}{L_r'} v_{rq} \end{cases} \tag{6}$$

where $R_r'$, $L_r'$ and $E_{dq}$ are given by

$$R_r' = R_r + \left(\frac{L_m}{L_s}\right)^2 R_s \tag{7}$$

$$L_r' = L_r - \frac{L_m^{\,2}}{L_s} \tag{8}$$

$$E_{dq} = \frac{L_m}{L_s}\left(v_{sdq} - j\omega_r\psi_{sdq} - \frac{R_s}{L_s}\psi_{sdq}\right) \tag{9}$$

The electromagnetic torque directly depends on stator flux and rotor current as

$$T_e = \frac{L_m}{L_s}\left(\psi_{sq} i_{rd} - \psi_{sd} i_{rq}\right) \tag{10}$$

The harmonic pollution of the output current in the GSC

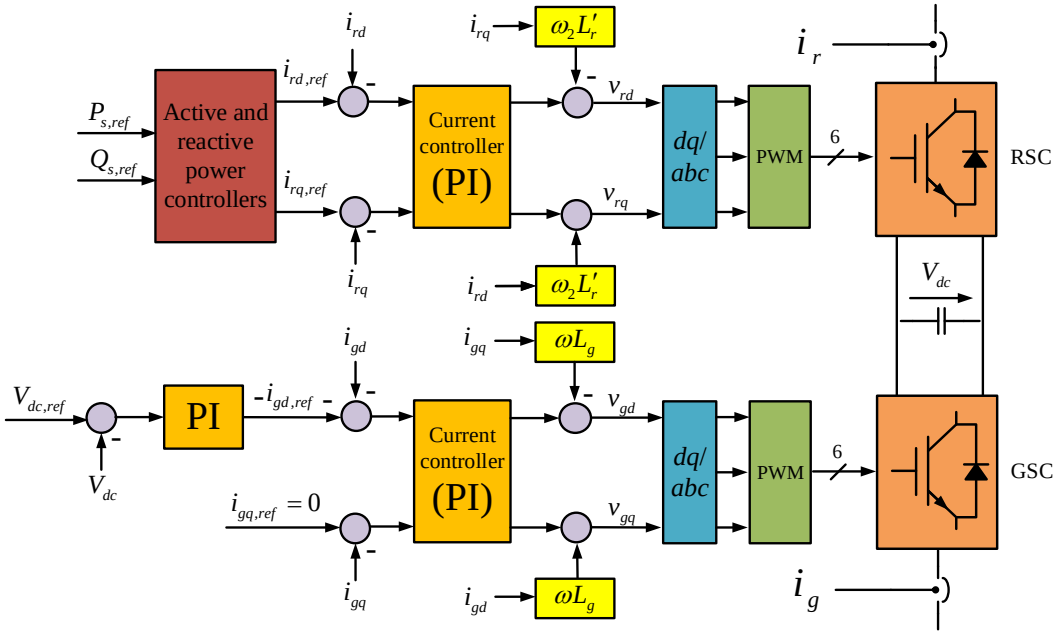


Fig. 2: Schematic diagram of PI controllers with PWM structure for RSC and GSC.

for an appropriate selected switching frequency is kept low enough by means of a filter. This filter which is located in the grid side is a series RL low pass filter which consists of $R_g$ and $L_g$. The state space representations of grid side filter are obtained as

$$\begin{cases} \dfrac{di_{gd}}{dt} = -\dfrac{\omega_b R_g}{L_g} i_{gd} + \omega_b \omega i_{gq} - \dfrac{\omega_b}{L_g} v_{sd} + \dfrac{\omega_b}{L_g} v_{gd} \\ \dfrac{di_{gq}}{dt} = -\dfrac{\omega_b R_g}{L_g} i_{gq} - \omega_b \omega i_{gd} - \dfrac{\omega_b}{L_g} v_{sq} + \dfrac{\omega_b}{L_g} v_{gq} \end{cases} \quad (11)$$

Considering synchronous reference frame with the $d$ axis aligned with the stator voltage space vector, the dynamic model of DC-link is described by the following instantaneous power balance.

$$CV_{dc} \frac{dV_{dc}}{dt} = -P_r - v_{sd} i_{gd} - P_{loss} \quad (12)$$

Fig. 2 shows the conventional control system of RSC and GSC. In the RSC, the $d$ and $q$ components of rotor current reference value are generated using active and reactive power controllers. The difference between these reference components and measured values of rotor current are applied to the current controller. $v_{rd}$ and $v_{rq}$ are obtained from the current controller and converted to $abc$ quantities. Then, IGBT gate drive signals are generated using PWM switching technique.

The control system in GSC keeps the DC-link voltage constant as its main purpose. Taking into consideration the vector control oriented with stator voltage, $i_{gd,ref}$ controls the DC-link voltage. Reactive power which is injected into the power grid by GSC can be stated as

$$Q_g = Im\left\{v_{sdq} i^*_{gdq}\right\} = v_{sq} i_{gd} - v_{sd} i_{gq} \quad (13)$$

Accordingly, the reactive power is controlled by $i_{gq,ref}$ and can be injected into the grid. In this study, we set $Q_{g,ref} = 0$.

## Review of SMC for Fault Ride Through

SMC is a nonlinear control technique with several advantages such as simplicity, robustness against system uncertainties and disturbances originated from external source, as well as good dynamical response. The SMC structure consists of equivalent control vector obtained in regard to the system mathematical model and switching part of control vector. In the SMC method, sliding surfaces are defined and the system states are pushed to their desired values. In [28], the sliding surfaces for RSC control have been considered the error between the measured and reference rotor currents as follows:

$$\begin{cases} s_{rd} = i_{rd,ref} - i_{rd} \\ s_{rq} = i_{rq,ref} - i_{rq} \end{cases} \quad (14)$$

The equivalent rotor voltages are obtained by supposing the sliding surface derivatives to be zero.

$$\begin{cases} \dfrac{ds_{rd}}{dt} = \dfrac{di_{rd,ref}}{dt} - \dfrac{di_{rd}}{dt} \\ \dfrac{ds_{rq}}{dt} = \dfrac{di_{rq,ref}}{dt} - \dfrac{di_{rq}}{dt} \end{cases} \quad (15)$$

The equivalent values of rotor voltages obtained by substituting (6) into (15) are stated as follows.

$$\begin{cases} v_{rd}^{eq} = \dfrac{L_r'}{\omega_b}\dfrac{di_{rd,ref}}{dt} + \left(R_r' i_{rd} - \omega_2 L_r' i_{rq} + E_d\right) \\ v_{rq}^{eq} = \dfrac{L_r'}{\omega_b}\dfrac{di_{rq,ref}}{dt} + \left(R_r' i_{rq} + \omega_2 L_r' i_{rd} + E_q\right) \end{cases} \quad (16)$$

The switching rotor voltages are properly designed so that the derivative of Lyapunov function, which is considered as $V = \frac{1}{2} s_i^2$ , $i = rd, rq$ , becomes negative-definite as follows:

$$\begin{cases} v_{rd}^{s} = k_{rd}\, sign\left(s_{rd}\right) & , k_{rd} \text{ is positive} \\ v_{rq}^{s} = k_{rq}\, sign\left(s_{rq}\right) & , k_{rq} \text{ is positive} \end{cases} \quad (17)$$

The rotor voltage consists of two parts: the equivalent value and the switching value given as

$$\begin{cases} v_{rd} = v_{rd}^{eq} + v_{rd}^{s} \\ v_{rq} = v_{rq}^{eq} + v_{rq}^{s} \end{cases} \quad (18)$$

Fig. 3 depicts the schematic diagram of the SMC used in the RSC control structure which has been proposed in [28]. It is adjusted according to equations in per unit values that have been presented in this paper.

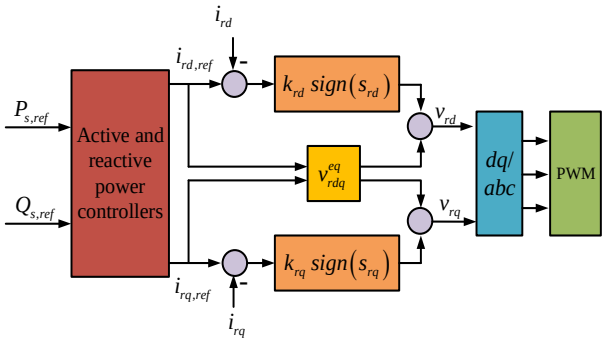


Fig. 3: Schematic diagram of the SMC used in RSC control structure.

In the GSC control structure, SMC sets the $dq$ components of the GSC current by considering state space representations of the grid side filter, (11), and thus, defining sliding surfaces as follows:

$$\begin{cases} s_{gd} = i_{gd,ref} - i_{gd} \\ s_{gq} = i_{gq,ref} - i_{gq} \end{cases} \quad (19)$$

$$\begin{cases} \dfrac{ds_{gd}}{dt} = \dfrac{di_{gd,ref}}{dt} - \dfrac{di_{gd}}{dt} \\ \dfrac{ds_{gq}}{dt} = \dfrac{di_{gq,ref}}{dt} - \dfrac{di_{gq}}{dt} \end{cases} \quad (20)$$

$$\begin{cases} v_{gd}^{eq} = \dfrac{L_g}{\omega_b}\dfrac{di_{gd,ref}}{dt} + \left(R_g i_{gd} - \omega L_g i_{gq} + v_{sd}\right) \\ v_{rq}^{eq} = \dfrac{L_g}{\omega_b}\dfrac{di_{gq,ref}}{dt} + \left(R_g i_{gq} + \omega L_g i_{gd} + v_{sq}\right) \end{cases} \quad (21)$$

$$\begin{cases} v_{gd}^{s} = k_{gd}\, sign\left(s_{gd}\right) & , k_{gd} \text{ is positive} \\ v_{gq}^{s} = k_{gq}\, sign\left(s_{rq}\right) & , k_{gq} \text{ is positive} \end{cases} \quad (22)$$

$$\begin{cases} v_{gd} = v_{gd}^{eq} + v_{gd}^{s} \\ v_{gq} = v_{gq}^{eq} + v_{gq}^{s} \end{cases} \quad (23)$$

The block diagram of the SMC applied to the GSC, which has been proposed in [28], has been adjusted based on equations in per unit values within this paper (see Fig. 4).

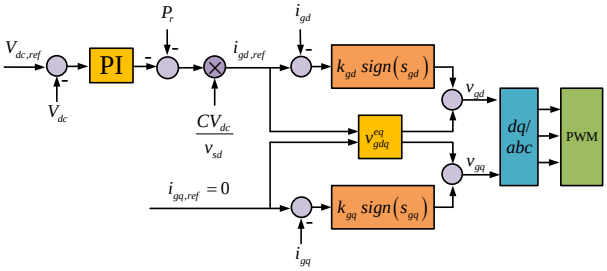


Fig. 4: Schematic diagram of the SMC used in GSC control structure.

## The Proposed Predictive Approach

The MPC schemes for electromagnetic torque and current control in RSC and DC-link voltage and current control in GSC, which are on the basis of system models for predicting the action of state variables at the next sampling time and generating switching drive signals of power converters, are presented in this section. Firstly, the predicted value of a state variable is computed for all switching states which can exist. Then, the appropriate switching state which minimizes a cost function is chosen. Considering the discrete nature of power converters, the finite number of switching states, and the fast microprocessors, online minimization of the cost function is possible [31], [32]. It is essential to note that stability analysis of MPC controlled power converters has been presented in [33], [34] by considering the cost function of MPC as a candidate Lyapunov function. Fig. 5 illustrates the schematic diagram of the proposed MPC-based controllers' design for RSC and GSC.

### *A. MPC-Based Control of RSC*

Fig. 6 shows an RSC that is assumed to be a three-phase converter with two power switches for each phase. At any specific time, only one switch is permitted to operate. The switching signals $S_a$ , $S_b$ , and $S_c$ can be defined as

$$S_a = \begin{cases} 1 & if\ \ S_1\ \ on\ \ and\ \ S_4\ \ off \\ 0 & if\ \ S_1\ \ off\ \ and\ \ S_4\ \ on \end{cases} \quad (24)$$

$$S_b = \begin{cases} 1 & if\ \ S_2\ \ on\ \ and\ \ S_5\ \ off \\ 0 & if\ \ S_2\ \ off\ \ and\ \ S_5\ \ on \end{cases} \quad (25)$$

$$S_c = \begin{cases} 1 & if\ \ S_3\ \ on\ \ and\ \ S_6\ \ off \\ 0 & if\ \ S_3\ \ off\ \ and\ \ S_6\ \ on \end{cases} \quad (26)$$

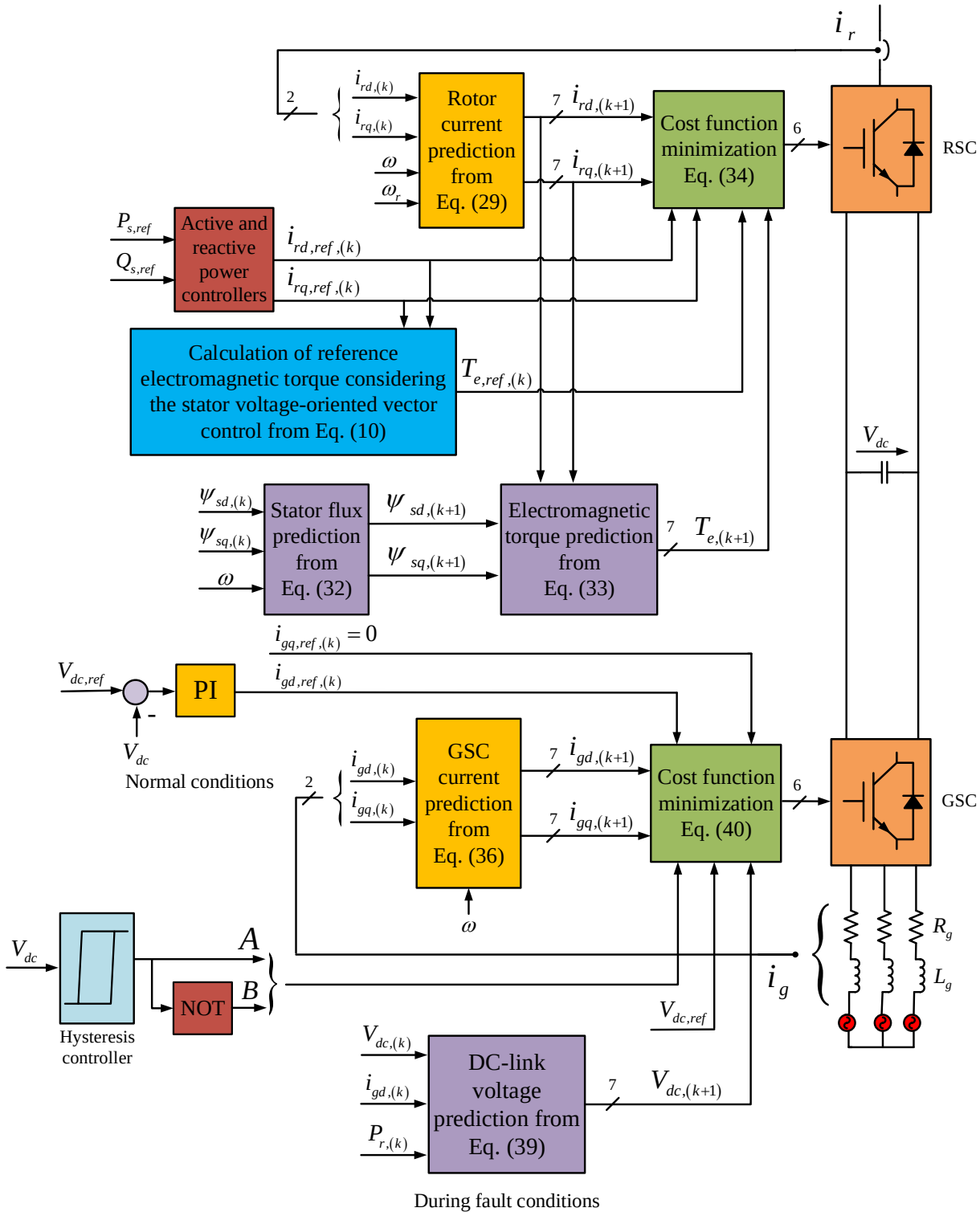


Fig. 5: Schematic diagram of the improved MPC implemented in RSC and GSC control structures.

The switching states of the three-phase two-level converter shown in Fig. 6 are given in Table 1. The converter's output voltage vector is described as follows:

$$\boldsymbol{v} = \frac{2}{3}\left(v_{aN} + \boldsymbol{a}v_{bN} + \boldsymbol{a}^2 v_{cN}\right) \quad (27)$$

where $\boldsymbol{a} = e^{j2\pi/3}$, and $v_{iN} = S_i V_{dc}$; $i = a,b,c$. Considering the possible combinations of switching signals, eight states and consequently seven different vectors of voltage are achieved (i.e. the switching states 1 and 8 in Table 1 present similar voltage vector which have been written in red.). In order to predict the action of $dq$ components of rotor current, a discrete-time model in sampling time $T_s$ is used which is obtained by a simple approximation of the derivatives. Forward Euler

approximation method is used to approximate the $dq$ components of rotor current derivative as follows:

$$\begin{cases} \dfrac{di_{rd}}{dt} \approx \dfrac{i_{rd,(k+1)} - i_{rd,(k)}}{T_s} \\ \dfrac{di_{rq}}{dt} \approx \dfrac{i_{rq,(k+1)} - i_{rq,(k)}}{T_s} \end{cases} \quad (28)$$

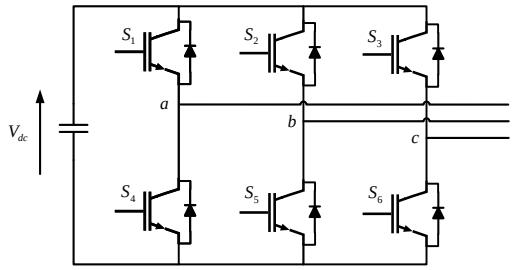


Fig. 6: Three-phase power converter circuit.

Table 1: Switching states of the three-phase two-level converter

| | $S_1$ | $S_2$ | $S_3$ | $S_4$ | $S_5$ | $S_6$ |
|---|---|---|---|---|---|---|
| **1** | 0 | 0 | 0 | 1 | 1 | 1 |
| **2** | 0 | 0 | 1 | 1 | 1 | 0 |
| **3** | 0 | 1 | 0 | 1 | 0 | 1 |
| **4** | 0 | 1 | 1 | 1 | 0 | 0 |
| **5** | 1 | 0 | 0 | 0 | 1 | 1 |
| **6** | 1 | 0 | 1 | 0 | 1 | 0 |
| **7** | 1 | 1 | 0 | 0 | 0 | 1 |
| **8** | 1 | 1 | 1 | 0 | 0 | 0 |

By replacement of (28) into (6), the $dq$ components of rotor current at the next sampling time are given by

$$\begin{cases} i_{rd,(k+1)} = T_s\left(-\dfrac{\omega_b R'_r}{L'_r} i_{rd,(k)} + \omega_b \omega_2 i_{rq,(k)} - \dfrac{\omega_b}{L'_r} E_{d,(k)} + \dfrac{\omega_b}{L'_r} v_{rd,(k)}\right) + i_{rd,(k)} \\ i_{rq,(k+1)} = T_s\left(-\dfrac{\omega_b R'_r}{L'_r} i_{rq,(k)} - \omega_b \omega_2 i_{rd,(k)} - \dfrac{\omega_b}{L'_r} E_{q,(k)} + \dfrac{\omega_b}{L'_r} v_{rq,(k)}\right) + i_{rq,(k)} \end{cases} \quad (29)$$

The above equations are utilized for calculating a cost function which is given in the following paragraphs; it is defined so as to minimize the quadratic error between reference values of rotor current components and their predicted values. For simplicity, the reference rotor currents are considered not to change during each sampling time; thus:

$$i_{rd,ref,(k+1)} \approx i_{rd,ref,(k)},\ i_{rq,ref,(k+1)} \approx i_{rq,ref,(k)} \quad (30)$$

Similar principle is used in predictive electromagnetic torque control. In other words, predictions are made for the future values of the stator flux and electromagnetic torque in this scheme. Forward Euler approximation is also considered to compute the $dq$ components of the stator flux as follows:

$$\begin{cases} \dfrac{d\psi_{rd}}{dt} \approx \dfrac{\psi_{rd,(k+1)} - \psi_{rd,(k)}}{T_s} \\ \dfrac{d\psi_{rq}}{dt} \approx \dfrac{\psi_{rq,(k+1)} - \psi_{rq,(k)}}{T_s} \end{cases} \quad (31)$$

The stator flux components at the next sampling time are calculated by substituting (31) into (5).

$$\begin{cases} \psi_{sd,(k+1)} = T_s \omega_b \left(v_{sd,(k)} - R_s i_{sd,(k)} + \omega \psi_{sq,(k)}\right) + \psi_{sd,(k)} \\ \psi_{sq,(k+1)} = T_s \omega_b \left(v_{sq,(k)} - R_s i_{sq,(k)} - \omega \psi_{sd,(k)}\right) + \psi_{sq,(k)} \end{cases} \quad (32)$$

Given the values of stator flux and rotor current components at the next sampling time and substituting them into (10), the electromagnetic torque prediction is obtained:

$$T_{e,(k+1)} = \frac{L_m}{L_s}\left(\psi_{sq,(k+1)} i_{rd,(k+1)} - \psi_{sd,(k+1)} i_{rq,(k+1)}\right) \quad (33)$$

Similar to reference rotor currents, the reference electromagnetic torque at the next sampling time is assumed to be equal with the present sampling time.

The switching state is selected corresponding to minimum cost function for the next sampling time, and hence applied to RSC in order to achieve an appropriate electromagnetic torque and rotor current regulation. The cost function is defined as:

$$g_1 = \alpha\left[\left(i_{rd,ref,(k)} - i_{rd,(k+1)}\right)^2 + \left(i_{rq,ref,(k)} - i_{rq,(k+1)}\right)^2\right] + \beta\left[\left(T_{e,ref,(k)} - T_{e,(k+1)}\right)^2\right] \quad (34)$$

where, $\alpha$ and $\beta$ are weighting factors and in this paper have been assigned 0.3 and 0.7, respectively by trial and error to improve both transient rotor current and transient electromagnetic torque during fault conditions. Due to the dependence of the electromagnetic torque on the rotor current, the rotor current can be indirectly controlled by controlling the electromagnetic torque. Hence, the weighting factor of electromagnetic torque term is considered to be larger than the weighting factor of the rotor current term in the (34). Based on [32], weighting factors are design parameters and adjusting of these factors depends on terms of the cost function. In other words, each term in the cost function is multiplied by a weighting factor to allow balancing of the different units and magnitudes of the controlled variables and to control their relative importance. A systematic way to determine these parameters is still a challenge and an open topic for research.

*B. MPC-Based Control of GSC*

Similar to RSC topology, GSC is considered to be a three-phase two-level converter with seven different vectors of voltage (Fig. 6). GSC current action is predicted by following approximation equations regarding to current derivative $dq$ components:

$$\begin{cases} \dfrac{di_{gd}}{dt} \approx \dfrac{i_{gd,(k+1)} - i_{gd,(k)}}{T_s} \\ \dfrac{di_{gq}}{dt} \approx \dfrac{i_{gq,(k+1)} - i_{gq,(k)}}{T_s} \end{cases} \quad (35)$$

The predicted components of GSC current are obtained by substituting (35) into (11) as

$$\begin{cases} i_{gd,(k+1)} = T_s\left(-\dfrac{\omega_b R_g}{L_g} i_{gd,(k)} + \omega_b \omega i_{gq,(k)} - \dfrac{\omega_b}{L_g} v_{sd,(k)} + \dfrac{\omega_b}{L_g} v_{gd,(k)}\right) + i_{gd,(k)} \\ i_{gq,(k+1)} = T_s\left(-\dfrac{\omega_b R_g}{L_g} i_{gq,(k)} - \omega_b \omega i_{gd,(k)} - \dfrac{\omega_b}{L_g} v_{sq,(k)} + \dfrac{\omega_b}{L_g} v_{gq,(k)}\right) + i_{gq,(k)} \end{cases} \quad (36)$$

Since DC-link dynamics is nonlinear, the conventional PI control for DC-link voltage regulation will fail to operate properly considering uncertainties and voltage dips. Hence, during fault conditions, predictive DC-link voltage control is designed based on DC-link dynamics equation (12) regardless of GSC switching losses as follows:

$$CV_{dc}\frac{dV_{dc}}{dt} = -P_r - v_{gd} i_{gd} \quad (37)$$

Based on forward Euler approximation, the derivative of DC-link voltage can be written as

$$\frac{dV_{dc}}{dt} \approx \frac{V_{dc,(k+1)} - V_{dc,(k)}}{T_s} \quad (38)$$

The predicted DC-link voltage is calculated by substituting (38) into (37).

$$V_{dc,(k+1)} = T_s\left(-\frac{P_{r,(k)}}{CV_{dc}} - \frac{v_{gd,(k)} i_{gd,(k)}}{CV_{dc}}\right) + V_{dc,(k)} \quad (39)$$

Similar to MPC scheme in RSC, changes of the reference values in one sampling time are ignored.

The switching state of GSC is obtained on the basis of the defined cost function (40) in order to return the minimum value for the next sample time:

$$g_2 = A\left(V_{dc,ref} - V_{dc,(k+1)}\right)^2 + B\left(i_{gd,ref,(k)} - i_{gd,(k+1)}\right)^2 + \left(i_{gq,ref,(k)} - i_{gq,(k+1)}\right)^2 \quad (40)$$

As shown in Fig. 5, $A$ and $B$ are obtained from a hysteresis controller which its output takes zero or one values. It should be noted that according to the nominal value of $V_{dc}$ (i.e. 1150 V) the upper and lower bands of the hysteresis controller have been considered 1165 V and 1155 V, respectively. When the DC-link voltage exceeds the upper band, the output value of the hysteresis controller will be one. If the DC-link voltage is less than the lower limit, the output value of the hysteresis controller is zero. In fact, at normal conditions the cost function (40) is the quadratic error between reference values of GSC current components and their predicted values. Whereas, during fault conditions, this cost function becomes the summation of the quadratic error between $q$ component of predicted GSC current and its reference, and the quadratic error between predicted DC-link voltage and its reference.

## Results and Discussion

The test system shown in Fig. 1 is modeled and simulated in the MATLAB-SIMULINK environment to investigate the performance of the proposed approach in FRT capability of the grid-connected DFIG-based WT with regard to the U.S. grid code stated by the Federal Energy Regulatory Commission, FERC. Fig. 7 shows the voltage dip ride through curve as specified by the FERC grid code. Accordingly, WTs must provide FRT support and remain connected to power grid in fault conditions with 85% depth and 600 ms duration in the point of common coupling (PCC) voltage [6]. In this study, the proposed control objectives are to restrict the current of rotor winding and the DC-link voltage to the ranges of 2 pu and 1.2 times of DC-link rated voltage value, respectively [35].

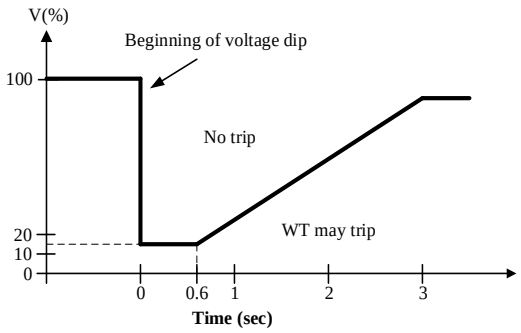


Fig. 7: Low voltage ride through (LVRT) requirement presented by FERC.

Parameters of the power grid, synchronous generator and DFIG-based WT shown in Fig. 1 are given in Tables 2-4. At time t=1 s, a 600 ms three-phase short-circuit fault has been simulated in the transmission line, which drops the PCC voltage to 15% of its rated value. Fig. 8 shows the transient response of DFIG-based WT during the fault.

Simulations are performed for a constant wind speed equal to 12 m/s. Results are compared with PI control and SMC methods which utilize PWM to implement the desired control.

For proper impartial comparison between conventional PWM and switching based on MPC theory, the same average of switching frequency has been considered in the latter one. Rotor current and DC-link voltage intense transients can be seen as the fault occurs and as it is cleared. When the conventional PI method is used, at the fault occurrence moment, the rotor current reaches 3.5 pu as a consequence of the magnetic coupling between stator and rotor.

Table 2: Parameters of electrical power grid

| | | | | |
|---|---|---|---|---|
| Rated voltage | | | | 25 kV |
| Rated frequency | | | | 60 Hz |
| Parameters of transmission lines | | | | |
| | Sequences | | | |
| | Positive | | | Zero |
| $R$(Ω / km) | 0.1153 | | | 0.413 |
| $L$(mH / km) | 1.05 | | | 3.32 |
| $C$(nF / km) | 11.33 | | | 5.01 |
| | # 1 | # 2 | # 3 | # 4 |
| Length(km) | 20 | 15 | 15 | 30 |
| Parameters of loads | | | | |
| | $P$(kW) | | | $Q$(kVAr) |
| # 1 | 400 | | | 120 |
| # 2 | 600 | | | 150 |

Table 3: Parameters of synchronous generator

| | |
|---|---|
| Rated voltage | 400 V |
| Rated power | 85 kVA |
| Rated speed | 1500 rpm |
| $X_d$ | 1.305 pu |
| $X_d'$ | 0.296 pu |
| $X_d''$ | 0.252 pu |
| $X_q$ | 0.474 pu |
| $X_q''$ | 0.243 pu |
| $X_l$ | 0.18 pu |
| $T_d'$ | 1.01 s |
| $T_d''$ | 0.053 s |
| $T_{qo}''$ | 0.1 s |
| Stator resistance | $2.8544 * 10^{-3}$ pu |
| Pole pairs | 4 |
| Inertia coefficient | 3.2 s |

Table 4: Parameters of WT with DFIG

| | |
|---|---|
| Rated power | 1.5 MW |
| Rated value of $v_s$ | 575 V |
| Rated frequency | 60 Hz |
| $T_s$ | $5 * 10^{-6}$ s |
| Nominal wind speed | 12 m/s |
| $R_s$ | 0.00706 pu |
| $R_r$ | 0.005 pu |
| Leakage inductance of stator | 0.1716 pu |
| Leakage inductance of rotor | 0.156 pu |
| $L_m$ | 2.9 pu |
| Pole pairs | 3 |
| Inertia constant | 0.685 s |
| $R_g$ | 0.003 pu |
| Filter reactance in grid side | 0.3 pu |
| Nominal value of $V_{dc}$ | 1150 V |
| $C$ | 10 mF |

Furthermore, the sudden voltage drop prevents GSC from delivering the excess power to the power grid. Therefore, the excess power in RSC causes DC-link voltage fluctuations to exceed their permissible limit (around 1.4 pu in this case). Accordingly, there is the risk of damage to RSC and DC-link capacitor. SMC method can limit the DC-link over-voltage bellow 1.2 times of DC-link rated voltage value, but it is incapable to restrict the rotor current within permissible limits. However, using the proposed method, peak oscillations of DC-link voltage and rotor current will be restricted to acceptable thresholds and ride through capability of DFIG-based WT will be ensured. Significant mechanical stresses are created due to electromagnetic torque fluctuations under low grid voltage conditions which consequently reduce the machine reliability. The performance of the proposed method in electromagnetic torque peak suppression can be observed in Fig. 8c. As shown in Figs. 8d and 8e, output active and reactive powers of DFIG-based WT by using the proposed method have better transient responses than PI control and SMC methods, especially at the fault clearance time.

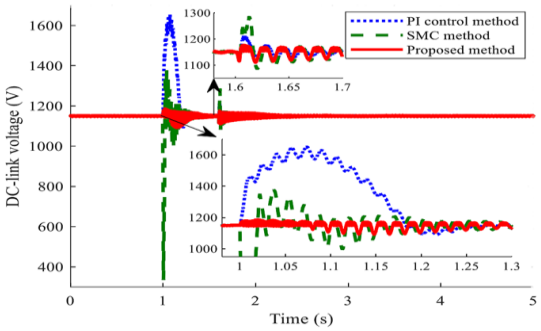


(a)

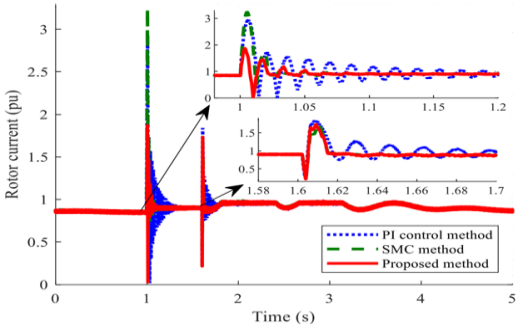


(b)

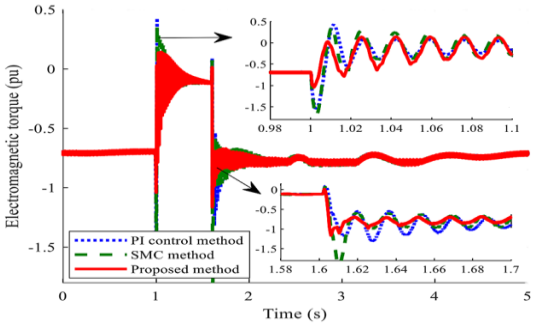


(c)

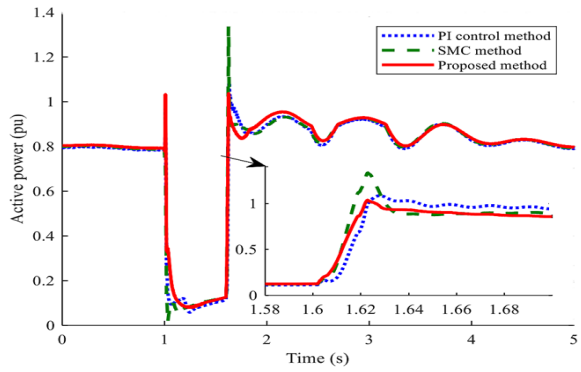


(d)

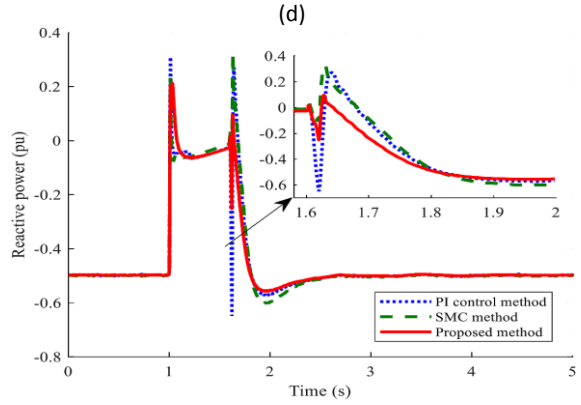


(e)

Fig. 8: Transient behavior of DFIG-based WT under wind speed of 12 m/s and an 85% three-phase fault: (a) DC-link voltage (V); (b) rotor current (pu); (c) electromagnetic torque (pu); (d) active power (pu); (e) reactive power (pu).

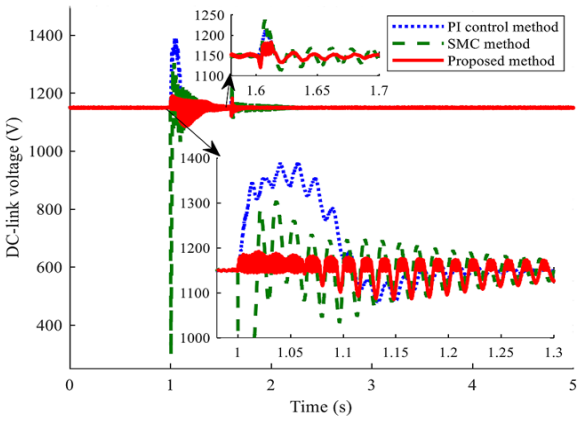


(a)

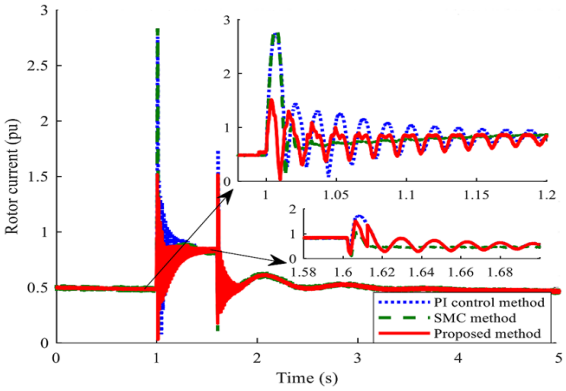


(b)

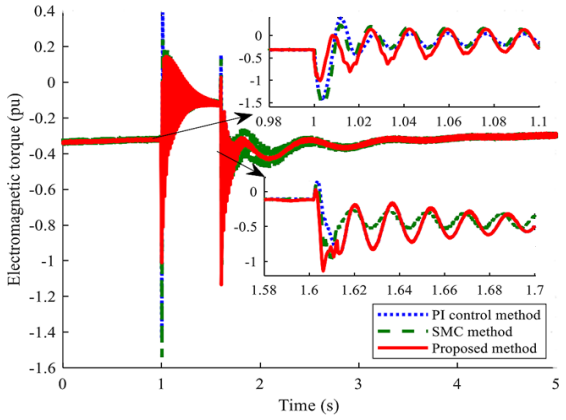


(c)

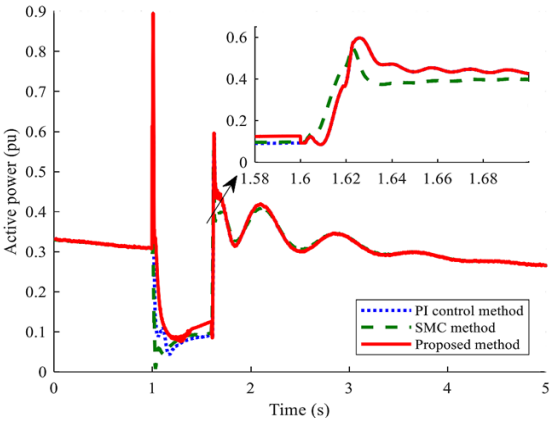


(d)

### *A. Operation with Variable Wind Speed*

In order to prove the effectiveness of the proposed MPC-based control approach considering the variability of wind speed, three other case studies are conducted in this part.

A three-phase fault occurs such that it leads to 85% voltage dip.

The simulated fault is cleared after 600 ms. Transient behavior of DFIG-based WT using wind speeds of 7 and 10 m/s are shown in Figs. 9 and 10, respectively.

Also, in order to investigate real wind turbulence in action, variable wind speed firstly starts with 12 m/s; then at time t=10 s a real turbulence term which is generated by Dryden velocity spectra [36] is applied.

The wind speed variations and its effects on transient behavior of DFIG-based WT are illustrated in Figs. 11 and 12, respectively. It is observed from Figs. 9, 10, and 12 that the SMC method cannot limit the rotor current to 2 pu, but it keeps the DC-link voltage within the permissible range.

Also, the proposed FRT enhancement approach is capable to constrain the DC-link voltage, rotor current and electromagnetic torque within specified bounds, and thus, the FRT capability of DFIG-based WT is improved.

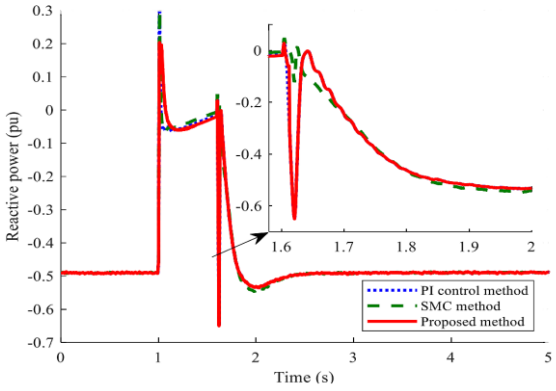


(e)

Fig. 9: Transient behavior of DFIG-based WT under wind speed of 7 m/s and an 85% three-phase fault: (a) DC-link voltage (V); (b) rotor current (pu); (c) electromagnetic torque (pu); (d) active power (pu); (e) reactive power (pu).

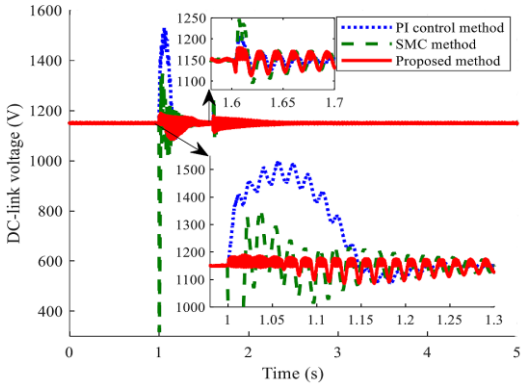


(a)

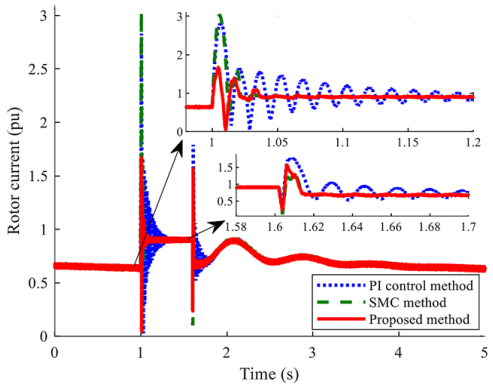


(b)

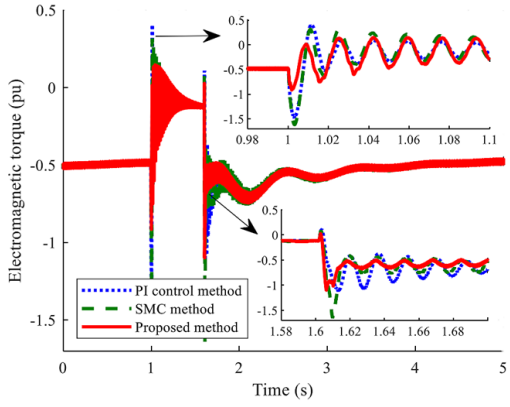


(c)

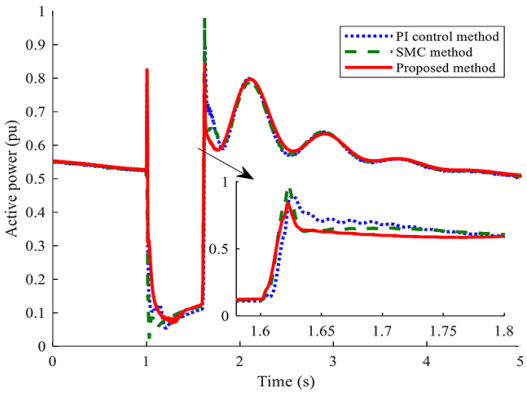


(d)

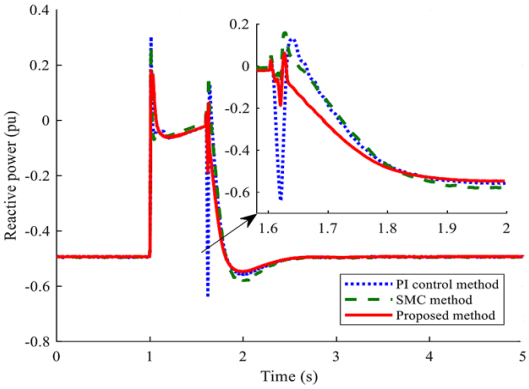


(e)

Fig. 10: Transient behavior of DFIG-based WT under wind speed of 10 m/s and an 85% three-phase fault: (a) DC-link voltage (V); (b) rotor current (pu); (c) electromagnetic torque (pu); (d) active power (pu); (e) reactive power (pu).

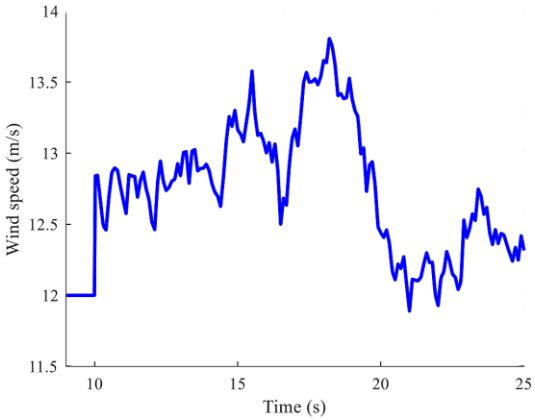


Fig. 11: Wind profile (m/s).

### *B. Operation with Single-Phase Fault*

A short-circuit fault of single-phase to ground is tested to examine the robustness of the improved MPC schemes for enhancing FRT capability. Given the DFIG-based WT operating under wind speed of 12 m/s, the performance of coordinated MPC approach is compared to PI control and SMC methods which is shown in Fig. 13. The proposed method improves the peak DC-link voltage, rotor current, and electromagnetic torque by 5.53%, 35.33%, and 83.75%, respectively, and reduces

their corresponding oscillations in comparison with the results derived from PI and SMC applications for FRT capability enhancement.

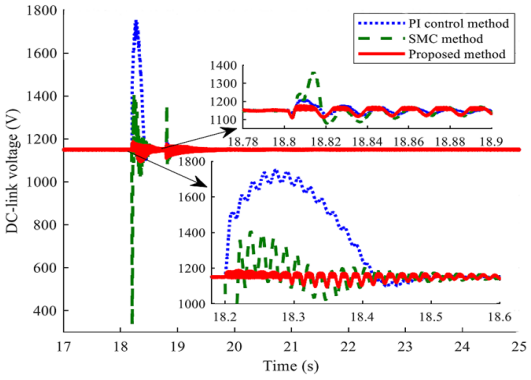


(a)

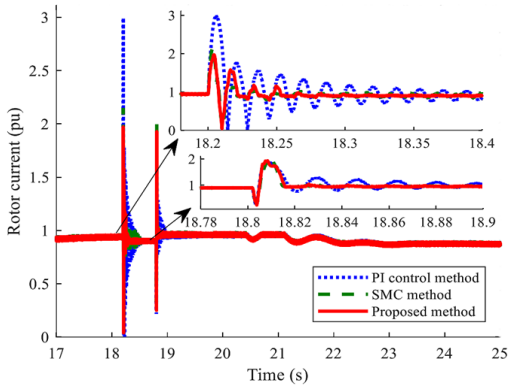


(b)

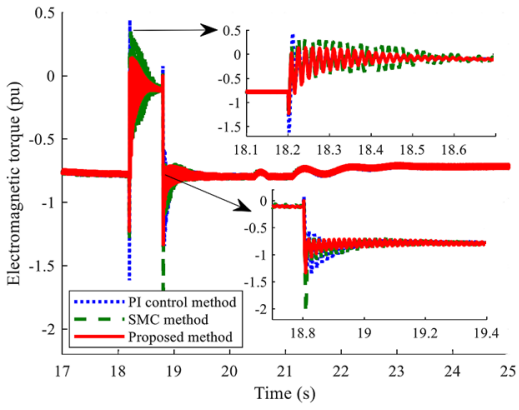


(c)

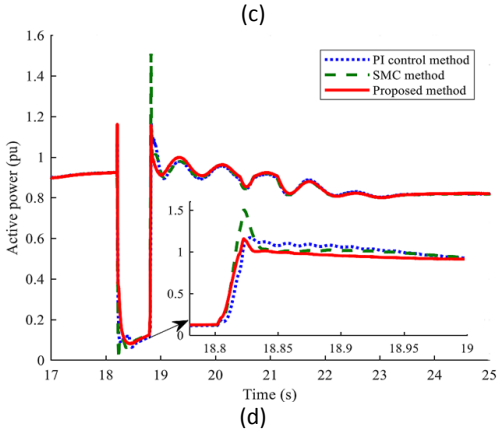


(d)

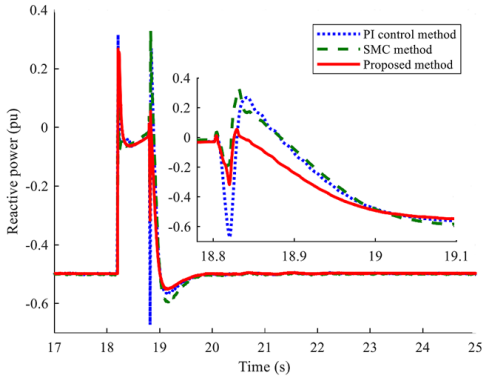


(e)

Fig. 12: Transient behavior of DFIG-based WT under variable wind speed and an 85% three-phase fault: (a) DC-link voltage (V); (b) rotor current (pu); (c) electromagnetic torque (pu); (d) active power (pu); (e) reactive power (pu).

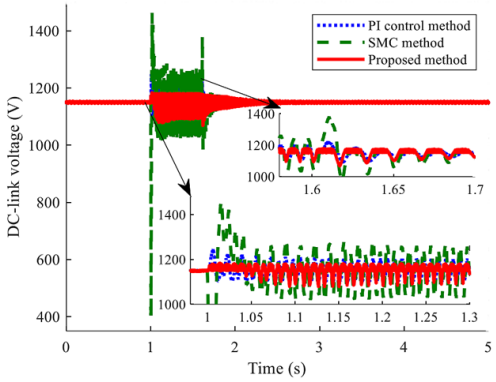


(a)

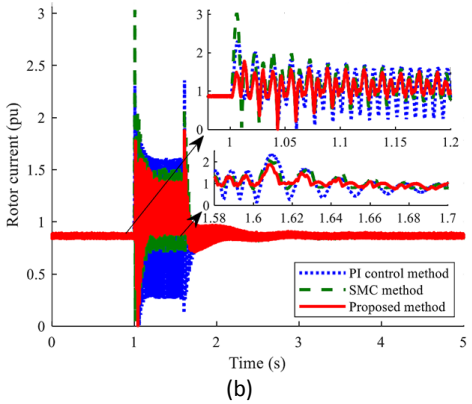


(b)

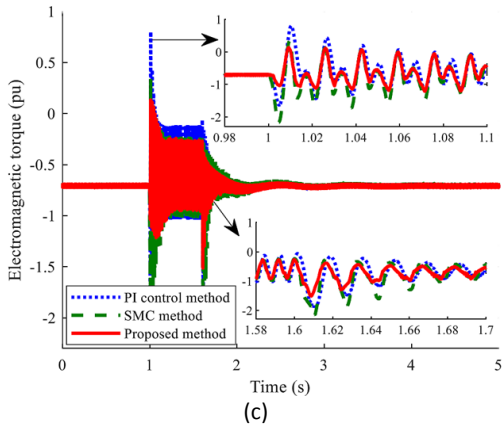


(c)

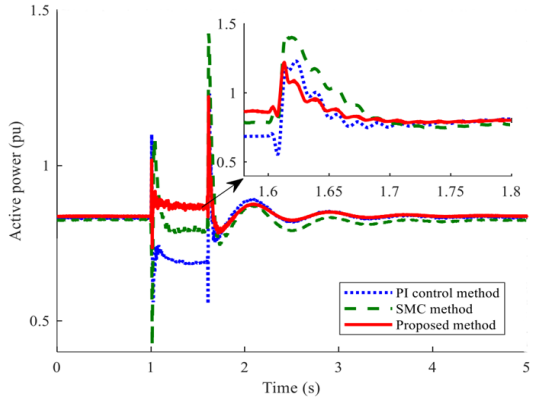


(d)

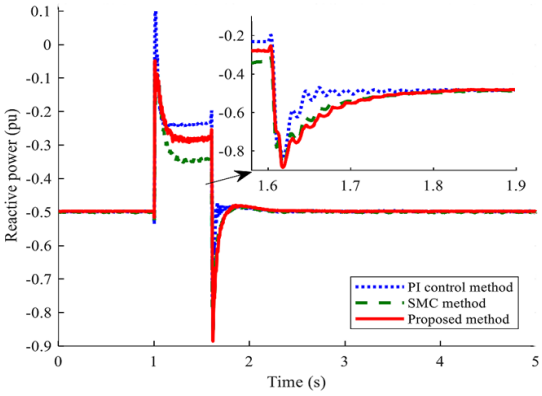


(e)

Fig. 13: Transient behavior of DFIG-based WT under wind speed of 12 m/s and single-phase fault: (a) DC-link voltage (V); (b) rotor current (pu); (c) electromagnetic torque (pu); (d) active power (pu); (e) reactive power (pu).

### *C. Operation with Variation in DFIG Parameters*

In this part, the simulation is performed when the magnetizing inductance, stator and rotor resistances are 1.5 and 0.5 times of their nominal values to investigate robust performance of the proposed control method against parameter uncertainties [21]. Figs. 14 and 15 depict the simulation results. In such cases, where DFIG parameters vary, the proposed MPC-based control scheme is more effective than both of the PI control and SMC methods in terms of FRT enhancement.

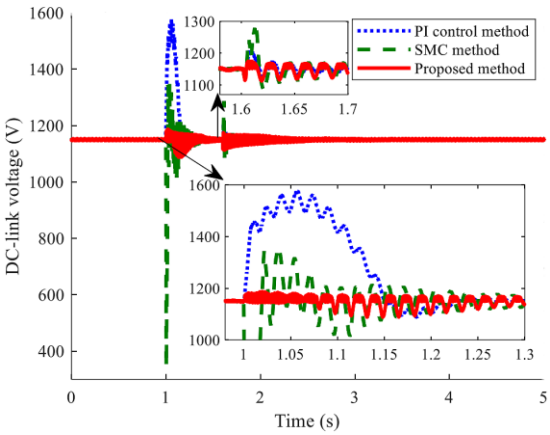


(a)

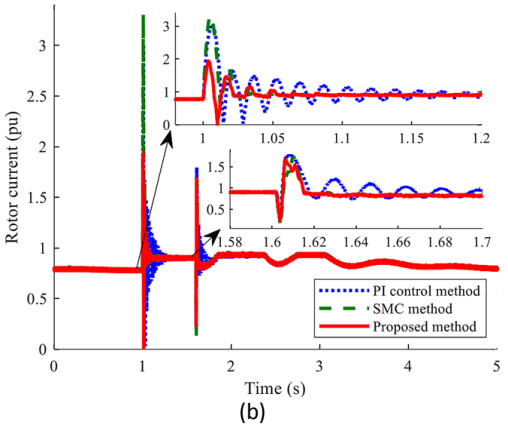


(b)

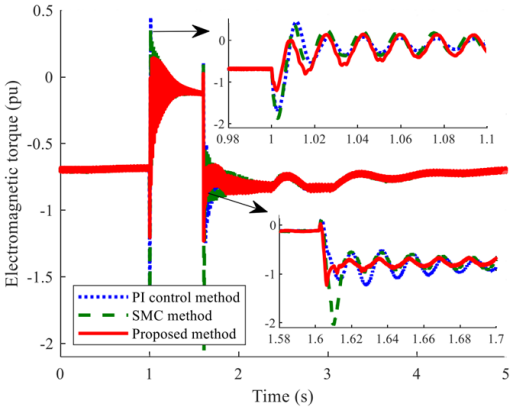


(c)

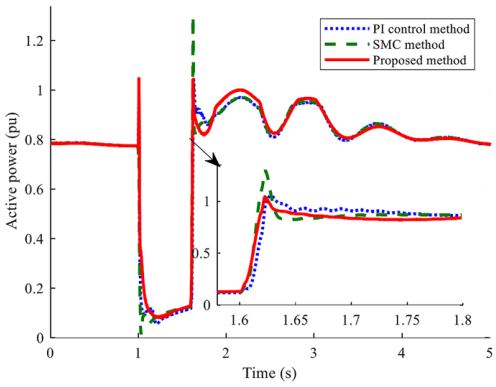


(d)

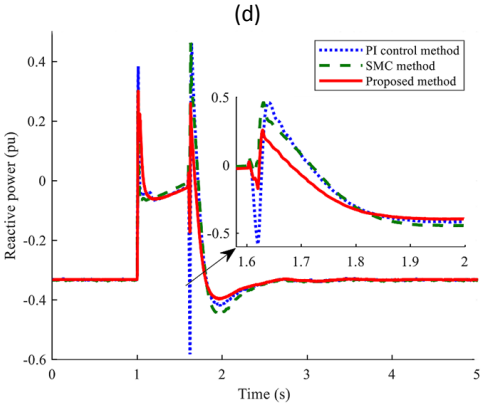


(e)

Fig. 14: Transient behavior of DFIG-based WT under wind speed of 12 m/s, an 85% three-phase fault and DFIG parameter variation: $R_s \rightarrow 1.5R_s$ , $R_r \rightarrow 1.5R_r$ , $L_m \rightarrow 1.5L_m$ ; (a) DC-link voltage (V); (b) rotor current (pu); (c) electromagnetic torque (pu); (d) active power (pu); (e) reactive power (pu).

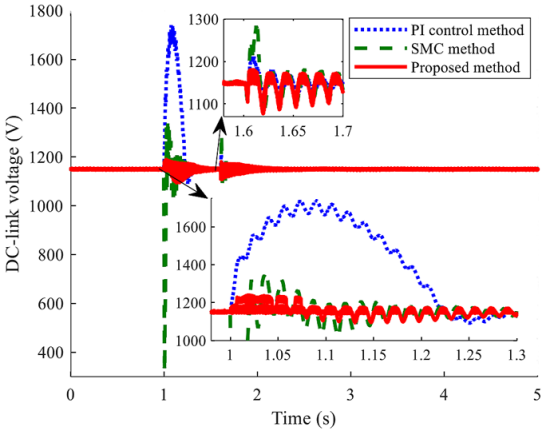


(a)

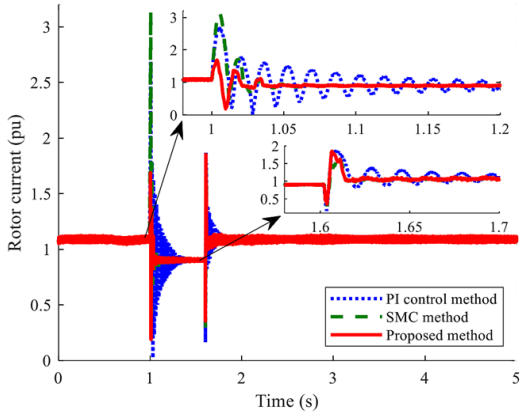


(b)

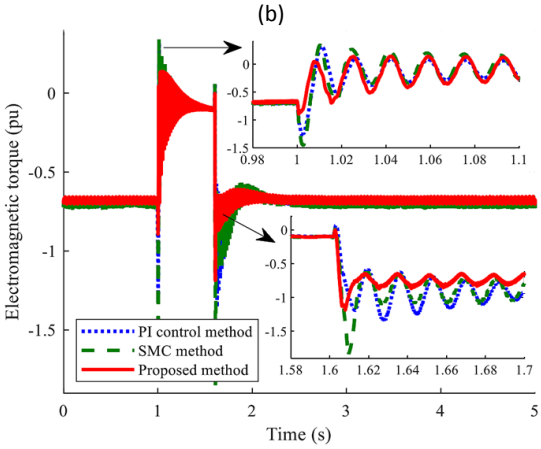


(c)

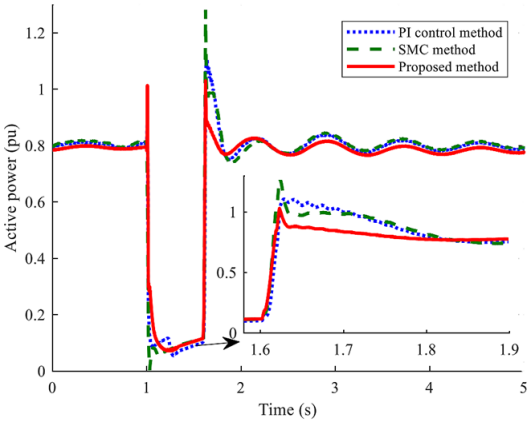


(d)

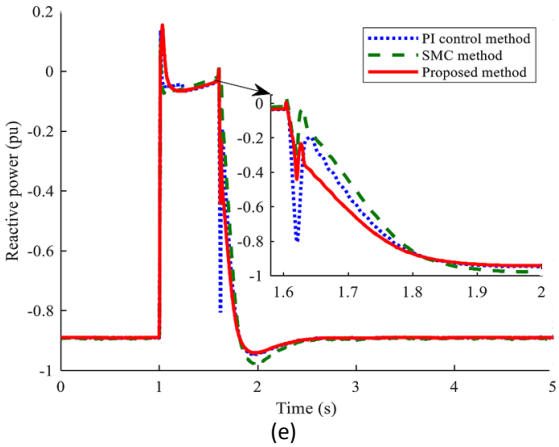


(e)

Fig. 15: Transient behavior of DFIG-based WT under wind speed of 12 m/s, an 85% three-phase fault and DFIG parameter variation: $R_s \rightarrow 0.5R_s$, $R_r \rightarrow 0.5R_r$, $L_m \rightarrow 0.5L_m$; (a) DC-link voltage (V); (b) rotor current (pu); (c) electromagnetic torque (pu); (d) active power (pu); (e) reactive power (pu).

### *D. Operation with a Severe Three-Phase Fault*

In order to study the DFIG transient behavior under a severe three-phase fault using the proposed method, a 90% three-phase dip in voltage is considered. In Fig. 16, simulation results show that using the coordinated MPC approach, the peak rotor current, electromagnetic torque and DC-link voltage are limited significantly.

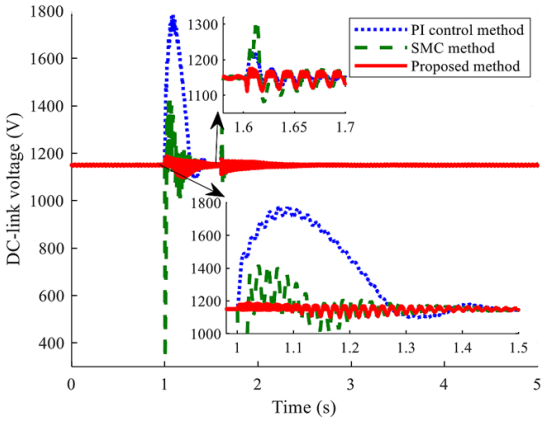


(a)

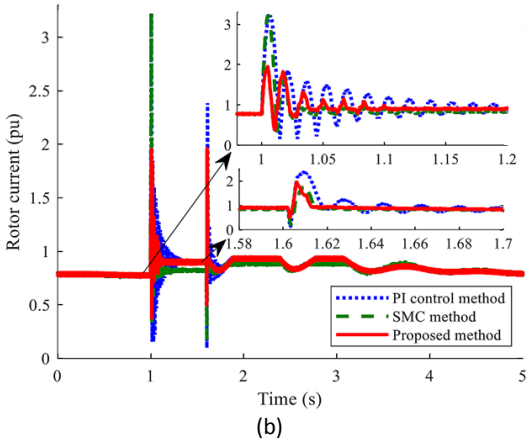


(b)

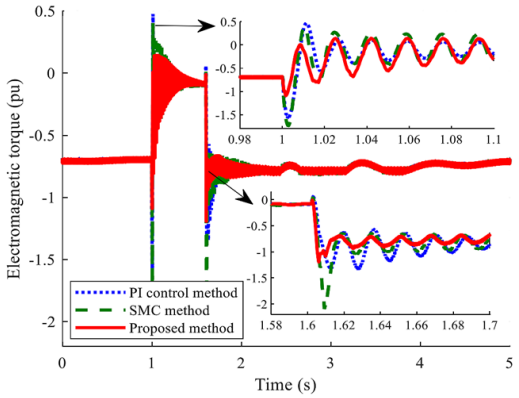


(c)

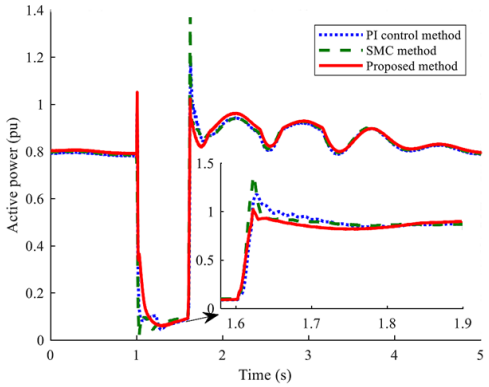


(d)

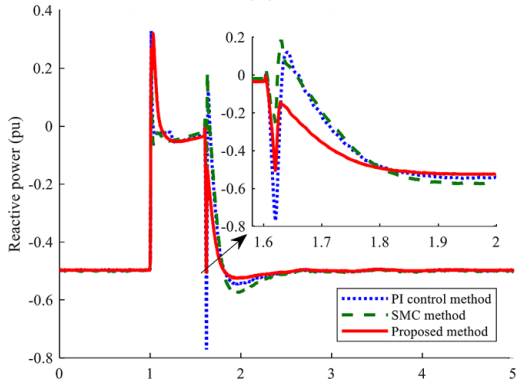


(e)

Fig. 16: Transient behavior of DFIG-based WT under wind speed of 12 m/s and a 90% three-phase fault: (a) DC-link voltage (V); (b) rotor current (pu); (c) electromagnetic torque (pu); (d) active power (pu); (e) reactive power (pu).

From the above different case studies provided in this section, it can be observed that, using the proposed method, the DC-link voltage and the rotor current are kept within acceptable limits. Moreover, it is worth noticing the fast dynamic behavior of the proposed method. This can be explained by the fact that MPC is a direct strategy that does not require an inner PI control loop for modulators. Hence, there is no bandwidth limitation for the electromagnetic torque dynamics. Although the proposed control scheme requires lots of calculations compared to conventional methods, fortunately, the today performance of modern microprocessors is sufficiently high to make this approach practical.

## Conclusion

This paper proposed a novel MPC-based control strategy to improve the FRT capability of grid-connected DFIG-based WTs. Simulation results illustrated that the proposed control scheme is able to effectively reduce the peak values of DC-link voltage, rotor current and electromagnetic torque, while maintaining their values within the acceptable threshold. As a consequence of the inherent fast dynamics of the proposed control method, it also reduces system oscillations during fault conditions. Accordingly, the DFIG-based WT successfully rides through grid faults and provides continuous active/reactive power for the grid during and post faults without requiring any auxiliary hardware protection devices, ensuring the compliance to grid code requirements.

Finally, the robustness, effectiveness, and proper operation of the proposed control strategy over PI control and SMC techniques with PWM switching algorithm was demonstrated by conducting several different case study simulations including: variable wind speeds, severe voltage dips, single-phase faults, and DFIG parameters variations. It should be noted that maximum peak values of DC-link voltage by using PI control, SMC and the proposed methods in different case studies were 1783, 1463 and 1190 V, respectively. The PI control, SMC and the proposed methods provided 3.23, 3.3 and 1.95 pu values, respectively as maximum peak of rotor current. Also, the maximum peak values of electromagnetic torque by using PI control, SMC and the proposed MPC strategies were 0.8, 0.4 and 0.14 pu, respectively. To conclude, the proposed model predictive approach can be considered as a fast, robust and effective FRT crowbarless solution for grid-connected DFIG-based WTs.

## Author Contributions

Z. Dehghani Arani, Prof. S. A. Taher, and M. H. Karimi proposed and designed the improved predictive control approach for DFIG-based wind turbine. Z. Dehghani Arani, and M. H. Karimi collected the data and wrote the original draft of the manuscript. Prof. S. A. Taher, and Z. Dehghani Arani carried out the data analysis. Prof. S. A. Taher, and Dr. M. Rahimi interpreted the results as well as reviewed and edited the manuscript.

## Acknowledgment

The authors gratefully acknowledge the vice-chancellor for research and technology of University of Kashan for the supports.

## Conflict of Interest

The authors declare that there is no conflict of

interests regarding the publication of this manuscript. In addition, the ethical issues, including plagiarism, informed consent, misconduct, data fabrication and/or falsification, double publication and/or submission, and redundancy have been completely observed by the authors.

## Abbreviations

| | |
|---|---|
| $\alpha$ , $\beta$ | Weighting factors |
| $\psi$ | Flux |
| $\omega$ | $dq$ reference frame's speed |
| $\omega_b$ | Base value of angular frequency (in this study, we considered $\omega = \omega_b$) |
| $\omega_r$ | Rotor speed |
| $\omega_2 = \omega - \omega_r$ | Rotor slip frequency |
| $A$ , $B$ | Zero or one values obtained from the hysteresis controller |
| ANFIS | Adaptive neuro-fuzzy inference system |
| $C$ | DC-link capacitance |
| DFIG | Doubly fed induction generator |
| DVR | Dynamic voltage restorer |
| $e$ | Error between the measured and reference values of parameters |
| $E$ | Rotor back-EMF voltage |
| FRT | Fault ride through |
| $g_1$, $g_2$ | Cost functions in RSC and GSC control structures respectively |
| GSC | Grid side converter |
| $i$ | Current |
| $k$ | SMCs' parameters |
| $L_g$ | Filter inductance used in grid side |
| $L_m$ | Magnetizing inductance |
| $L_r$ | Self-inductance of rotor |
| $L'_r$ | Transient inductance |
| $L_s$ | Self-inductance of stator |
| LVRT | Low voltage ride through |
| MPC | Model predictive control |
| $P$ | Active power |
| PCC | Point of common coupling |
| PI | Proportional-plus-integral |
| $P_{loss}$ | Total conducting and switching losses of the GSC |
| $P_r$ | Rotor instantaneous input power |
| PWM | Pulse-width modulation |
| $Q$ | Reactive power |
| $R_g$ | Filter resistance used in grid side |
| $R_r$ | Resistance of rotor |
| $R'_r$ | Transient resistance |
| $R_s$ | Resistance of stator |
| RSC | Rotor side converter |
| $s$ | Sliding surfaces |
| $S_a$ , $S_b$ , $S_c$ | Switching signals |
| SC | Superconducting coil |
| SFCL | Superconducting fault current limiter |
| SMC | Sliding mode control |
| SMES-FCL | Superconducting magnetic energy storage-fault current limiter |
| STATCOM | Static synchronous compensator |
| SVC | Static volt ampere reactive compensator |
| $T_e$ | Electromagnetic torque |
| $T_s$ | Sampling time |
| $v$ | Voltage |
| $V_{dc}$ | DC-link voltage |
| WECS | Wind energy conversion system |
| WT | Wind turbine |

**Subscripts**

| | |
|---|---|
| $d$, $q$ | Synchronous $dq$ reference frame |
| $g$ | Quantities of grid side filter |
| $(k)$ | Quantities at the $k^{th}$ sampling time (present sampling time) |
| $(k+1)$ | Quantities at the $k+1^{th}$ sampling time (next sampling time) |
| $nominal$ | Nominal quantity |
| $r$ | Quantities of rotor |
| $ref$ | Reference quantities |
| $s$ | Quantities of stator |

**Superscripts**

| | |
|---|---|
| $eq$ | Equivalent control inputs |
| $s$ | Switching control inputs |

## References


[1] E. J. N. Menezes, A. M. Araújo, N. S. B. da Silva, "A review on wind turbine control and its associated methods," J. Clean. Prod., 174: 945-953, 2018.

[2] M. J. Morshed, A. Fekih, "A new fault ride-through control for DFIG-based wind energy systems," Electr. Power Syst. Res., 146: 258-269, 2017.

[3] J. Morren, S. W. H. de Haan, "Ridethrough of wind turbines with doubly-fed induction generator during a voltage dip," IEEE Trans. Energy Convers., 20(2): 435-441, 2005.

[4] S. Wang, N. Chen, D. Yu, A. Foley, L. Zhu, K. Li, J. Yu, "Flexible fault ride through strategy for wind farm clusters in power systems with high wind penetration," Energy Convers. Manage., 93(3): 239-248, 2015.

[5] A. Jalilian, S. B. Naderi, M. Negnevitsky, M. Tarafdar Hagh, K. M. Muttaqi, "Low voltage ride-through enhancement of DFIG-based wind turbine using DC link switchable resistive type fault current limiter," Electr. Power Energy Syst., 86: 104-119, 2017.

[6] M. Tsili, S. Papathanassiou, "A review of grid code technical requirements for wind farms," IET Renew. Power Gen., 3(3): 308-332, 2009.

[7] D. Campos-Gaona, E. L. Moreno-Goytia, O. Anaya-Lara, "Fault ride-through improvement of DFIG-WT by integrating a two-degrees-of-freedom internal model control," IEEE Trans. Ind. Electron., 60(3): 1133-1145, 2013.

[8] W. Chen, D. Xu, N. Zhu, M. Chen, F. Blaabjerg, "Control of doubly fed induction generator to ride through recurring grid faults," IEEE Trans. Power Electron., 31(7): 4831-4846, 2016.

[9] X. Xiao, R. Yang, X. Chen, Z. Zheng, C. Li, "Enhancing fault ride-through capability of DFIG with modified SMES-FCL and RSC control," IET Gener. Transmiss. Distrib., 12(1): 258-266, 2018.

[10] S. I. Gkavanoudis, C. S. Demoulias, "Fault ride-through capability of a DFIG in isolated grids employing DVR and supercapacitor energy storage," Int. J. Electr. Power Energy Syst., 68: 356-363, 2015.

[11] Y. Kailasa Gounder, D. Nanjundappan, V. Boominathan, "Enhancement of transient stability of distribution system with SCIG and DFIG based wind farms using STATCOM," IET Renew. Power Gen., 10(8): 1171-1180, 2016.

[12] A. Safaei, B. Vahidi, S. H. Hosseinian, H. A. Abyaneh, "Fault ride-through capability improvement of doubly fed induction generator-based wind turbine using static volt ampere reactive compensator," AIP J. Renewable Sustainable Energy, 7(2), 2015.

[13] T. Karaipoom, I. Ngamroo, "Optimal superconducting coil integrated into DFIG wind turbine for fault ride through capability enhancement and output power fluctuation suppression," IEEE Trans. Sustain. Energy, 6(1): 28-42, 2015.

[14] S. Teimourzadeh, F. Aminifar, M. Davarpanah, J. M. Guerrero, "Macroprotections for microgrids: toward a new protection paradigm subsequent to distributed energy resource integration," IEEE Ind. Electron. Mag., 10(3): 6-18, 2016.

[15] S. B. Naderi, M. Negnevitsky, K. M. Muttaqi, "A modified DC chopper for limiting the fault current and controlling the DC-link voltage to enhance fault ride-through capability of doubly-fed induction-generator-based wind turbine," IEEE Trans. Ind. Appl., 55(2): 2021-2032, 2019.

[16] K. Du, X. Xiao, Y. Wang, Z. Zheng, C. Li, "Enhancing fault ride-through capability of DFIG-based wind turbines using inductive SFCL with coordinated control," IEEE Trans. Appl. Superconduct., 29(2): 1-6, 2019.

[17] Y. M. Alsmadi, L. Xu, F. Blaabjerg, A. J. P. Ortega, A. Y. Abdelaziz, A. Wang, Z. Albataineh, "Detailed investigation and performance improvement of the dynamic behavior of grid-connected DFIG-based wind turbines under LVRT conditions," IEEE Trans. Ind. Appl., 54(5): 4795-4812, 2018.

[18] M. J. Hossain, T. K. Saha, N. Mithulananthan, H. R. Pota, "Control strategies for augmenting LVRT capability of DFIGs in interconnected power system," IEEE Trans. Ind. Electron., 60(6): 2510-2522, 2013.

[19] D. Zhu, X. Zou, S. Zhou, W. Dong, Y. Kang, J. Hu, "Feedforward current references control for DFIG-based wind turbine to improve transient control performance during grid faults," IEEE Trans. Energy Convers., 33(2): 670-681, 2018.

[20] D. Xie, Z. Xu, L. Yang, J. Østergaard, Y. Xue, K. P. Wong, "A comprehensive LVRT control strategy for DFIG wind turbines with enhanced reactive power support," IEEE Trans. Power Syst., 28(3): 3302-3310, 2013.

[21] M. Rahimi, M. Parniani, "Transient performance improvement of wind turbines with doubly fed induction generators using nonlinear control strategy," IEEE Trans. Energy Convers., 25(2): 514-525, 2010.

[22] J. Liang, W. Qiao, R. G. Harley, "Feed-forward transient current control for low-voltage ride-through enhancement of DFIG wind turbines," IEEE Trans. Energy Convers., 25(3): 836-843, 2010.

[23] J. Liang, D. F. Howard, J. A. Restrepo, R. G. Harley, "Feed-forward transient compensation control for DFIG wind turbines during both balanced and unbalanced grid disturbances," IEEE Trans. Ind. Appl., 49(3): 1452-1463, 2013.

[24] A. J. Sguarezi Filho, E. R. Filho, "Model-based predictive control applied to the doubly-fed induction generator direct power control," IEEE Trans. Sustain. Energy, 3(3): 398-406, 2012.

[25] M. Soliman, O. P. Malik, D. T. Weswick, "Ensuring fault ride through for wind turbines with doubly fed induction generator: a model predictive control approach," in Proc. 18th IFAC World Conf.: pp. 1710-1715, 2011.

[26] M. Abdelrahem, M. H. Mobarak, R. Kennel, "Model predictive control for low-voltage ride through capability enhancement of DFIGs in variable-speed wind turbine systems," in Proc. of IEEE 9th Int. Conf. on Elect. and Computer Engineering,: 70-73, 2016.

[27] S. A. Taher, Z. Dehghani Arani, M. Rahimi, M. Shahidehpour, "Model predictive fuzzy control for enhancing FRT capability of DFIG-based WT in real-time simulation environment," Energy Syst., 9(4): 899-919, 2018.

[28] H. S. Naggar, A. S. Ahmed, M. M. Abd El-Aziz, "Low voltage ride through of doubly fed induction generator connected to the grid using sliding mode control strategy," Renew. Energy, 80: 583-594, 2015.

[29] S. A. Taher, Z. Dehghani Arani, M. Rahimi, M. Shahidehpour, "A new approach using combination of sliding mode control and feedback linearization for enhancing fault ride through capability of DFIG-based WT," Int. Trans. Electr. Energ. Syst., 28(10), 2018.

[30] M. Rahimi, "Coordinated control of rotor and grid sides converters in DFIG based wind turbines for providing optimal reactive power support and voltage regulation," Sustain. Energy Technol. Assess., 20: 47-57, 2017.

[31] S. Kouro, P. Cortes, R. Vargas, U. Ammann, J. Rodriguez, "Model predictive control-A simple and powerful method to control power converters," IEEE Trans. Ind. Electron., 56(6): 1826-1838, 2009.

[32] J. Rodriguez, P. Cortes, Predictive control of power converters and electrical drives, John Wiley & Sons, 2012.

[33] R. P. Aguilera, D. E. Quevedo, "On stability and performance of finite control set MPC for power converters," in Proc. Workshop Predictive Control Elect. Drives Power Electron.: 55-62, 2011.

[34] R. P. Aguilera, D. E. Quevedo, "Predictive control of power converters: Designs with guaranteed performance," IEEE Trans. Ind. Informat., 11(1): 53-63, 2015.

[35] A. H. Kasem, E. F. El-Saadany, H. H. El-Tamaly, M. A. A. Wahab, "An improved fault ride-through strategy for doubly fed induction generator-based wind turbines," IET Renew. Power Gener., 2(4): 201-214, 2008.

[36] C. K. Patel, H. T. Lee, I. M. Kroo, "Extracting energy from atmospheric turbulence," XXIX OSTIV Congress: 1-9, 2008.

## Biographies

**Zahra Dehghani Arani** (M'17) was born in Kashan, Isfahan, Iran, in 1990. She received both her B.Sc. and M.Sc. degrees in electrical engineering from the University of Kashan, Kashan, Iran, in 2012 and 2015, respectively. She is currently pursuing Ph.D. degree of power systems engineering at University of Kashan, Isfahan, Iran. Her current research interests include renewable energy, micro/smart grids, fuzzy expert systems, predictive control, nonlinear control, multi-agent systems, and applications of artificial intelligence and parallel computing in power engineering.

**Seyed Abbas Taher** (SM' 17) was born in Kashan, Isfahan, Iran, in 1964. He received his B.Sc. degree in electrical engineering from the Amirkabir University of Technology, Tehran, Iran in 1988, and his M.Sc. and Ph.D. degrees in electrical engineering from the Tarbiat Modares University, Tehran, Iran, in 1991 and 1997, respectively. In 1996, he joined the faculty of engineering, University of Kashan, where he has been a Full Professor since 2016. His current research interests include power system optimization and control design, analysis of electrical machines, power quality, and renewable energy.

**Mohammad Hossein Karimi** was born in Faridan, Isfahan, Iran, in 1986. He was graduated with B.Sc. degree in power electric engineering from the Islamic Azad University - Najaf Abad Branch, Isfahan, Iran in 2007. He received his M.Sc. degree in power electric engineering from University of Kashan, Isfahan, Iran in 2012. He's currently pursuing Ph.D. degree of power systems engineering at University of Kashan, Isfahan, Iran. His employment experience included the Iranian oil pipeline and telecommunication company, Tehran, Iran. His special fields of interest included microgrids and distribution systems.

**Mohsen Rahimi** is an Associate Professor at University of Kashan, Kashan, Iran. He received the B.Sc. degree in electrical engineering in 2001 from Isfahan University of Technology, Isfahan, Iran. He obtained both his M.Sc. and Ph.D. degrees in electrical engineering from Sharif University of Technology (SUT), Tehran, Iran, in 2003 and 2011, respectively.He worked for Saba Niroo, a wind turbine manufacturing company, during 2010–2011. His current research interests include modeling, control and stability analysis of power system dynamics with particular interest in control of grid-connected wind turbines, renewable energy sources, distributed generations, and AC/DC microgrids.



**How to cite this paper:**
Z. Dehghani Arani, S.A. Taher, M.H. Karimi, M. Rahimi, "Coordinated Model Predictive DC-Link Voltage, Current, and Electromagnetic Torque Control of Wind Turbine with DFIG under Grid Faults," Journal of Electrical and Computer Engineering Innovations, 8(2): 201-218, 2020.

**DOI:** 10.22061/JECEI.2020.7031.353

**URL:** http://jecei.sru.ac.ir/article_1465.html